Letter

Wave-particle duality in a quantum heat engine

Marcelo Janovitch,* Matteo Brunelli, and Patrick P. Potts†
Department of Physics and Swiss Nanoscience Institute, University of Basel, Klingelbergstrasse 82, 4056 Basel, Switzerland

(Received 31 March 2023; accepted 12 September 2023; published 5 October 2023)

According to the wave-particle duality (WPD), quantum systems show both particlelike and wavelike behavior and cannot be described using only one of these classical concepts. Identifying quantum features that cannot be reproduced by *any* classical means is key for quantum technology. This task is often pursued by comparing the quantum system of interest with a suitable classical counterpart. However, the WPD implies that a comparison with a single classical model is generally insufficient; at least one wave model and one particle model should be considered. Here we exploit this insight and contrast a bosonic quantum heat engine with two classical counterparts, one based on waves and one based on particles. While both classical models reproduce the average output power of the quantum engine, neither reproduces its fluctuations. The wave model fails to capture the vacuum fluctuations, while the particle model cannot reproduce bunching to its full extent. We find regimes where wave and particle descriptions agree with the quantum one, as well as a regime where neither classical model is adequate, revealing the role of the WPD in nonequilibrium bosonic transport.

DOI: 10.1103/PhysRevResearch.5.L042007

Introduction. The wave-particle duality (WPD) expresses the coexistence of particlelike and wavelike behavior in a single quantum system [1–3]. This fundamental principle, confirmed in both photon [4] and matter interferometers [3,5,6], is a pillar of our understanding of quantum mechanics. The WPD has been expressed in quantitative terms [7,8], extended to many-body interference [9], and even tested by interferometric scenarios in which neither particle nor wave models can describe the measurement outcomes [10].

Identifying genuine quantum behavior is central both for quantum technologies [11–15] and for fundamental aspects of quantum theory [16–20]. Generally, quantum behavior is identified by comparison with classical models. For instance, quantum computers are benchmarked by classical computers to identify a quantum advantage [21]. There is, however, no general recipe to determine the classical models that serve as a benchmark. Often, only a single classical model is considered, e.g., when results from quantum optics experiments are compared with predictions from classical electrodynamics [22]. However, the WPD implies that one model is not enough: To identify genuine quantum behavior, a system of bosons, for instance, should be benchmarked by both classical waves and particles. Otherwise, classical wave or particle phenomena may be misinterpreted as quantum signatures.

In this Research Letter, we exploit this insight from the WPD and contrast a minimal model of bosonic transport with two classical counterparts. We focus on a setup where quantum coherence is relevant: a pair of harmonic oscillators coupled coherently to each other and to thermal reservoirs at different temperatures (see Fig. 1). This system implements a quantum heat engine [23]; heat flowing from the hot bath to the cold bath gives rise to power output. We compare the quantum heat engine with two classical models, one in which bosons are modeled as waves (using classical Langevin equations) and one where bosons are modeled as particles (using a classical rate equation). Our classical wave and particle models should not be considered merely as approximations to the quantum model. Instead, they serve as benchmarks, to identify the departure from classical behavior.

Remarkably, both classical models reproduce the average power of the quantum model. However, both fail to reproduce fluctuations around this average. While the wave model cannot correctly describe vacuum fluctuations, the particle model does not result in the same amount of bunching as the quantum model. For both models, there are relevant limits where they accurately describe power fluctuations: The wave model becomes accurate in the high-temperature regime, where vacuum fluctuations do not matter; and the particle model becomes accurate for weak coupling, where the transport statistics becomes (bidirectional) Poissonian, as well as in the high-coupling regime, where the two oscillators effectively behave as a single one [24]. In these limits, power fluctuations can be described classically using *two* distinct models for the different limits. Away from these limits, the output power contains signatures of the WPD as neither waves nor particles can capture its fluctuations. Our results showcase that the WPD is a powerful tool to reveal the nonclassical features encoded in out-of-equilibrium quantum systems.

Quantum heat engine. We consider a quantum heat engine composed of two bosonic modes [24–26], with frequencies $\Omega_{h/c}$, described by the Hamiltonian

$$H(t) = \sum_{\alpha=h,c} \Omega_\alpha a_\alpha^\dagger a_\alpha + g(a_h^\dagger a_c e^{-i\Delta t} + a_c^\dagger a_h e^{i\Delta t}) \quad (1)$$

*m.janovitch@unibas.ch
†patrick.potts@unibas.ch

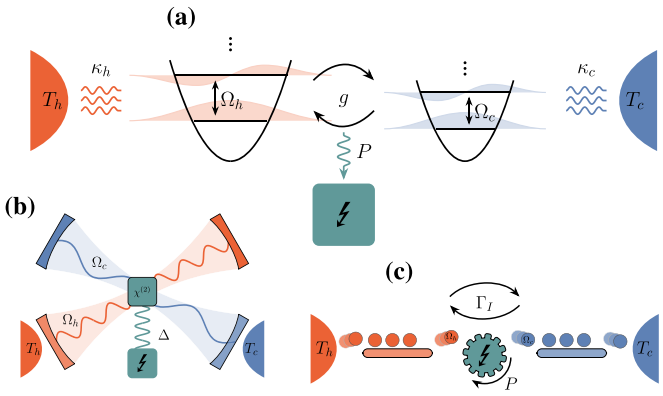

FIG. 1. (a) Schematic representation of the quantum heat engine. We consider two bosonic modes, described by the time-dependent Hamiltonian in Eq. (1), coupled to two thermal reservoirs. (b) Sketch of the wave model: Two classical waves interact by a $\chi^{(2)}$ nonlinear crystal, resulting in difference frequency generation. (c) Sketch of the particle model: Particles moving from a hot bath to a cold bath produce work by turning a gear, whereby they lose part of their energy.

in the Schrödinger picture. We work with units $\hbar = k_B = 1$ and $\Delta = \Omega_h - \Omega_c$. Each system mode is connected to a bath with different temperatures, and the heat flow leads to power output, $P(t) = -\partial_t H(t)$ [27], our quantity of interest. The setup is depicted in Fig. 1(a).

This model of a quantum heat engine can be realized in a superconducting circuit architecture [26,28–30]. In this case, each mode is provided by an *LC* resonator, the heat baths are provided by transmission lines, and the coupling between the modes is mediated by a Josephson junction. In this case, power is provided by a supercurrent against a voltage bias, due to photon-assisted Cooper-pair tunneling [26]. Another possible implementation of this engine is in optomechanical devices [31,32].

We are interested in the average power in the long-time limit, $\langle P\rangle_q$, and its zero-frequency noise,

$$\langle\langle P^2\rangle\rangle_q = 2\,\mathrm{Re}\int_0^\infty dt\,\langle\delta P(t)\delta P(0)\rangle_q, \tag{2}$$

with $\delta x := x - \langle x\rangle$, and at $t = 0$ we are at the long-time limit (or steady state in a suitable rotating frame [33]). We also introduced the subscript "q" to distinguish the quantum averages from the averages of the classical models in the following text. Equation (2) is directly connected to the variance of work [33]. Henceforth, we refer to it simply as *noise*.

The reduced system dynamics is described by the Lindblad master equation (LME),

$$\dot\rho = -i[H(t),\rho] + \sum_{\alpha=h,c}(\bar{\mathrm{n}}_\alpha + 1)\kappa_\alpha D[a_\alpha]\rho + \bar{\mathrm{n}}_\alpha\kappa_\alpha D[a_\alpha^\dagger]\rho, \tag{3}$$

with Bose-Einstein occupations $\bar{\mathrm{n}}_\alpha = (e^{\Omega_\alpha/T_\alpha} - 1)^{-1}$, $\bar{\mathrm{n}}_h \geqslant \bar{\mathrm{n}}_c$, and superoperators $D[L]\rho = L\rho L^\dagger - \frac{1}{2}\{L^\dagger L, \rho\}$. We note that due to the coherent coupling, the LME couples diagonal and off-diagonal elements of the density matrix in the particle number basis.

The LME (3) is equivalent to a set of *quantum* Langevin equations (QLEs), in the input-output formalism [34]

$$\dot a_h = -\Big(i\Omega_h + \frac{\kappa_h}{2}\Big)a_h - iga_c e^{-it\Delta} - \sqrt{\kappa_h}b_{h,\mathrm{in}}, \tag{4a}$$

$$\dot a_c = -\Big(i\Omega_c + \frac{\kappa_c}{2}\Big)a_c - iga_h e^{+it\Delta} - \sqrt{\kappa_c}b_{c,\mathrm{in}}, \tag{4b}$$

where the thermal baths are captured by input fields, $b_{\alpha,\mathrm{in}}$, and with *quantum* white noise autocorrelation function,

$$\langle b^\dagger_{\alpha,\mathrm{in}}(t')b_{\beta,\mathrm{in}}(t)\rangle_q = \bar{\mathrm{n}}_\alpha\delta_{\alpha\beta}\delta(t'-t), \tag{5}$$

with $[b_{\alpha,\mathrm{in}}(t'), b^\dagger_{\beta,\mathrm{in}}(t)] = \delta_{\alpha\beta}\delta(t'-t)$ and $\alpha,\beta = h,c$. This entails classical white noise *and* vacuum fluctuations, due to the bosonic algebra of the input fields. Moreover, the dynamics of any product of the ladder operators is computed through $(\dot{ab}) = \dot a b + a\dot b$.

In the long-time limit, the average power reduces to $\langle P\rangle_q = g\Delta\langle N_h - N_c\rangle_q$, with $N_\alpha = a^\dagger_\alpha a_\alpha$ and explicitly evaluated from a closed set of equations of motion, $\langle d/dt(a^\dagger_\alpha a_\beta)\rangle_q$; $\alpha,\beta = h,c$. The *same* equations of motion are obtained either from the LME (3) or from applying the QLEs (4) and the white noise autocorrelation functions (5). Armed with the equations of motion, noise (2) is evaluated by employing the quantum regression theorem and Wick's theorem [35]; details can be found in the Supplemental Material [33].

Wave heat engine. Our wave model, sketched in Fig. 1(b), consists of a pair of classical fields, externally driven by two thermal white noise sources. Formally, the model is based on the canonical association between the ladder operators and the complex amplitudes for the classical fields, $a_\alpha \leftrightarrow A_\alpha$. The classical dynamics is given by classical Langevin equations,

$$\dot A_h = -\Big(i\Omega_h + \frac{\kappa_h}{2}\Big)A_h - igA_c e^{-it\Delta} - \sqrt{\kappa_h}\xi_{h,\mathrm{in}}, \tag{6a}$$

$$\dot A_c = -\Big(i\Omega_c + \frac{\kappa_c}{2}\Big)A_c - igA_h e^{+it\Delta} - \sqrt{\kappa_c}\xi_{c,\mathrm{in}}. \tag{6b}$$

Above, the input fields encompass classical white noise, with

$$\langle\xi^*_{\alpha,\mathrm{in}}(t')\xi_{\beta,\mathrm{in}}(t)\rangle_w = \bar{\mathrm{n}}_\alpha\delta_{\alpha\beta}\delta(t'-t), \tag{7}$$

where we indicate the averages of the wave model with "w." Notably, $\xi_{\alpha,\mathrm{in}}$ are scalars and *commute*; thus the classical fields, A_α, are functions of the random inputs, $\xi_{\alpha,\mathrm{in}}$. A similar wave model has also been considered in Ref. [12] for unitary dynamics. We can visualize the wave model in a classical optical setting; see Fig. 1(b). Two cavities with frequencies Ω_α are supplied by thermal fluctuations, and a $\chi^{(2)}$ crystal amounts to difference frequency generation, producing a power-output field with frequency $\Delta = \Omega_h - \Omega_c$ [36,37].

In this case, the average power is given by $\langle P\rangle_w = g\Delta\langle|A_h|^2 - |A_c|^2\rangle_w$, and the average is taken with respect to classical white noise (7). The evaluation of power statistics closely follows those of the quantum model in the input-output formalism. From Eqs. (6) and the white noise relation (7), we compute $\langle d/dt(A^*_\alpha A_\beta)\rangle_w$, and a (classical) regression theorem [38] combined with Wick's or Isserlis's theorem [39] gives the noise. The procedure is carefully addressed in the Supplemental Material [33].

Particle heat engine. In our particle model, particles may reside on two different sites, as sketched in Fig. 1(c). The occupation numbers of those sites are governed by a classical

rate equation

$$\begin{aligned}\dot{p}_{n_h,n_c} &= \kappa_h(\bar{n}_h+1)(n_h+1)p_{n_h+1,n_c} + \kappa_h\bar{n}_h n_h p_{n_h-1,n_c} \\ &+ \kappa_c(\bar{n}_c+1)(n_c+1)p_{n_h,n_c+1} + \kappa_c\bar{n}_c n_c p_{n_h,n_c-1} \\ &+ \Gamma_I(n_h+1)n_c p_{n_h+1,n_c-1} + \Gamma_I(n_c+1)n_h p_{n_h-1,n_c+1} \\ &- \Gamma^0_{n_h,n_c} p_{n_h,n_c}, \end{aligned} \tag{8}$$

where p_{n_h,n_c} denotes the joint probability for the occupations n_h and n_c, the intrasystem jump rate is given by $\Gamma_I = 4g^2/(\kappa_h+\kappa_c)$, and the rate, $\Gamma^0_{n_h,n_c}$, is such that $\sum_{n_h,n_c}\dot{p}_{n_h,n_c} = 0$. We note that the rates for particles entering and leaving the system are the same as in the LME (3). Indeed, for $g=0$ the rate equation (8) coincides with the evolution of the diagonal elements of ρ given in Eq. (3). In contrast to the quantum model, transport within the system is described by incoherent jump processes, analogous to the jumps between the system and the baths. As sketched in Fig. 1(c), a particle moving from hot to cold will turn the gear in the orientation of the arrow and produce the work $\Omega_h - \Omega_c$. An opposite and less likely process is also allowed and would decrease the power output.

We find, in the long-time limit, $\langle P\rangle_p = \Gamma_I\Delta\langle n_h - n_c\rangle_p$, where $\langle x\rangle_p = \sum_{n_h,n_c} x(n_h,n_c)p_{n_h,n_c}$, resembling the behavior of the quantum model. In order to study the power fluctuations, we apply full counting statistics (FCS) [40] to Eq. (8). Concretely, we attach counting fields to intrasystem transitions and determine the particle current statistics [33].

Average power and noise. We find that the quantum, as well as the wave and particle models, lead to the same average power,

$$\begin{aligned}\langle P\rangle_q = \langle P\rangle_w = \langle P\rangle_p &= \frac{4g^2\kappa_h\kappa_c\Delta(\bar{n}_h-\bar{n}_c)}{(4g^2+\kappa_h\kappa_c)(\kappa_h+\kappa_c)} \\ &= \Delta(\bar{n}_h-\bar{n}_c)\big(\kappa_h^{-1}+\kappa_c^{-1}+\Gamma_I^{-1}\big)^{-1}, \end{aligned} \tag{9}$$

where the last equality illustrates an analogy to the addition of three conductances in series. For the wave model, the equality with the quantum one follows since only normal-ordered operators appear in computing the average power; thus vacuum fluctuations are irrelevant. For the particle model, we note that the steady-state power can be cast solely in terms of average number operators, $\langle P\rangle_q = g\Delta\langle N_h - N_c\rangle_q$, which are reproduced exactly by the particle model [33].

For each model, we find the power noise,

$$\langle\langle P^2\rangle\rangle_q = \mathcal{E}[\bar{n}_h(\bar{n}_h+1)+\bar{n}_c(\bar{n}_c+1)] - \mathcal{S}(\bar{n}_h-\bar{n}_c)^2, \tag{10a}$$

$$\langle\langle P^2\rangle\rangle_w = \mathcal{E}\big(\bar{n}_h^2+\bar{n}_c^2\big) - \mathcal{S}(\bar{n}_h-\bar{n}_c)^2, \tag{10b}$$

$$\langle\langle P^2\rangle\rangle_p = \mathcal{E}[\bar{n}_h(\bar{n}_h+1)+\bar{n}_c(\bar{n}_c+1)] - \mathcal{S}_p(\bar{n}_h-\bar{n}_c)^2, \tag{10c}$$

where we wrote our results in terms of equilibrium noise, $\mathcal{E}$, and shot noise, $\mathcal{S}$ ($\mathcal{S}_p$) [41]. The equilibrium noise,

$$\mathcal{E} = \frac{\langle P\rangle\Delta}{\bar{n}_h-\bar{n}_c}, \tag{11}$$

is proportional to the response coefficient in power when a temperature bias is applied, in agreement with the fluctuation-dissipation theorem [42]. For simplicity, we present shot noise in the case $\kappa_h = \kappa_c = \kappa$,

$$\mathcal{S} = \mathcal{E}\left[1 - 2g^2\frac{(4g^2+5\kappa^2)}{(4g^2+\kappa^2)^2}\right], \tag{12}$$

$$\mathcal{S}_p = \mathcal{S} + \mathcal{E}\frac{24g^4\kappa^2}{(6g^2+\kappa^2)(4g^2+\kappa^2)^2}. \tag{13}$$

General expressions for the noise can be found in the Supplemental Material [33].

The wave model reproduces the shot noise of the quantum model, but equilibrium fluctuations are reduced since the terms linear in $\bar{n}_\alpha$ are absent in Eq. (10b). These linear contributions stem from vacuum fluctuations and can be traced back to the quantum white noise autocorrelation function (5). This mismatch is shown in Fig. 2(a) (green-shaded region). While the wave model fails to capture the dominant contributions of noise at low temperatures, $\bar{n}_h, \bar{n}_c \lesssim 1$, it reproduces the quantum noise at high temperatures $\bar{n}_\alpha \gg 1$.

In contrast to the wave model, the particle model captures the equilibrium noise but fails to reproduce the shot noise of the quantum model. Indeed, as for the wave model, the quantum noise is an upper bound for the classical one since $(\mathcal{S}_p - \mathcal{S}) \geqslant 0$. Note that the terms linear in $\bar{n}_\alpha$, interpreted as vacuum fluctuations so far, are related to detailed balance in the particle model since $(\bar{n}_\alpha+1) = e^{\beta\Omega_\alpha}\bar{n}_\alpha$, leading to the same equilibrium noise. In Fig. 2(a) the red-shaded region illustrates the mismatch between the particle model and the quantum model, with a maximum mismatch at $g/\kappa = 1/2(1+\sqrt{3})^{1/2} \approx 2/3$. We observe that for both limits $g/\kappa \to 0$ and $g/\kappa \to \infty$ the particle model captures the noise of the quantum model, i.e., $\langle P\rangle_q = \langle P\rangle_p$ and $\langle\langle P^2\rangle\rangle_q = \langle\langle P^2\rangle\rangle_p$. For $g/\kappa_\alpha \to 0$, intersystem transitions provide a bottleneck, and transport exhibits bidirectional Poissonian statistics, fully characterized by the rates $\Gamma_{\alpha\beta} = \Gamma_I\bar{n}_\alpha(\bar{n}_\beta+1)$ [24],

$$\langle P\rangle_p = \Delta(\Gamma_{hc}-\Gamma_{ch}), \quad \langle\langle P^2\rangle\rangle_p = \Delta^2(\Gamma_{hc}+\Gamma_{ch}). \tag{14}$$

For $g/\kappa_\alpha \to \infty$ the system modes hybridize and effectively behave as a single oscillator in contact with two thermal baths [24,43]

$$\langle P\rangle_p = \frac{\kappa_c\kappa_h\Delta}{\kappa_c+\kappa_h}(\bar{n}_h-\bar{n}_c), \tag{15}$$

$$\begin{aligned}\langle\langle P^2\rangle\rangle_p = \frac{\kappa_c\kappa_h\Delta}{(\kappa_c+\kappa_h)^3}\big\{&(\kappa_c+\kappa_h)^2[\bar{n}_h(\bar{n}_h+1)+\bar{n}_c(\bar{n}_c+1)] \\ &- (\bar{n}_h-\bar{n}_c)^2\big(\kappa_h^2+\kappa_c^2\big)\big\}. \end{aligned} \tag{16}$$

To supplement the discussion of noise, we now analyze the Fano factor, $\mathcal{F} = \langle\langle P^2\rangle\rangle/(\langle P\rangle\Delta)$. This quantity is a measure of bunching and connected to intensity correlations [44,45]; for example, thermal light is (super-)Poissonian, $\mathcal{F} \geqslant 1$ (bunched), while the flux of single photons is sub-Poissonian (antibunched), $\mathcal{F} < 1$. For the quantum and particle models, we find $\mathcal{F}_q \geqslant \mathcal{F}_p \geqslant 1$, while the wave model can attain sub-Poissonian statistics since $\mathcal{F}_w$ can be both smaller and larger than 1, as exemplified in Figs. 2(b) and 2(c). To understand these results, we introduce $\delta\mathcal{F}_{qw(p)} = \mathcal{F}_q - \mathcal{F}_{w(p)}$, which represent the shaded regions in Figs. 2(b) and 2(c).

For the wave model, Eqs. (10a) and (10b) give $\delta\mathcal{F}_{qw} = (\bar{n}_h+\bar{n}_c)/(\bar{n}_h-\bar{n}_c)$. The divergence at equilibrium, $\bar{n}_h = \bar{n}_c$,

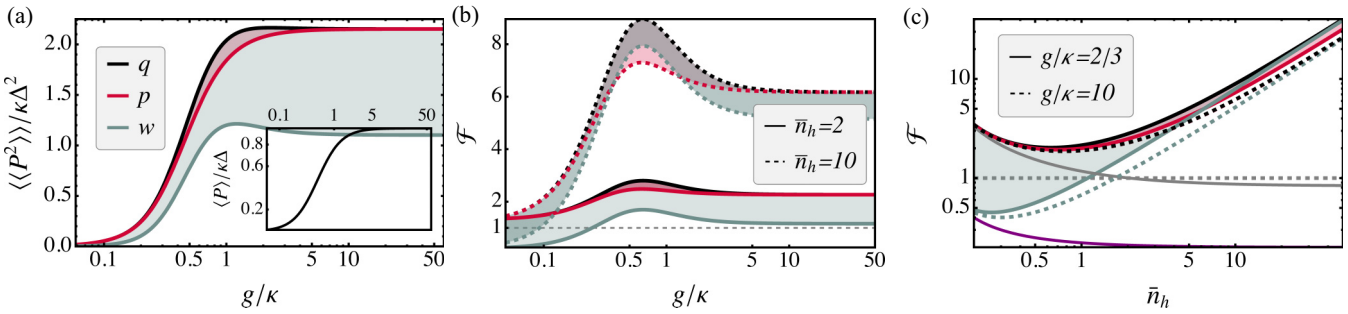

FIG. 2. Noise and the Fano factor. In all plots we set $\bar{n}_c = 0.1$, $\kappa_h = \kappa_c = \kappa$. (a) (linear-log) Power noise as a function of coupling between system modes, g/κ, and average power in the inset. We fixed $\bar{n}_h = 2$. The green-shaded (red-shaded) region indicates the mismatch between wave (particle) and quantum models; the particle model matches the quantum model for both small and large g/κ. (b) (linear-log) Fano factor as a function of g/κ, with $\bar{n}_h = 2$ (solid curves) and $\bar{n}_h = 10$ (dashed curves). For these temperatures, both classical models show a clear mismatch with the quantum one in the region where g is of the order of κ. The gray dashed line indicates $\mathcal{F} = 1$. (c) (log-log) Fano factor as a function of $\bar{n}_h$, with $g/\kappa = 2/3$ (solid curves) and $g/\kappa = 10$ (dashed curves). We see that for either coupling regime, the wave model converges to the quantum model for large $\bar{n}_h$. The gray dashed line indicates $\mathcal{F} = 1$, the solid gray curve is the bound provided by the TUR, and the purple curve is the bound from the modified TUR which holds for the wave model. We observe sub-Poissonian statistics for the wave model close for $\bar{n}_h \lesssim 1$.

is due to the absence of power, while equilibrium fluctuations are still present. We also note that in the high-temperature limit, $\delta\mathcal{F}_{qw}$ does not vanish, but $\mathcal{F}_{q(w)}$ are dominated by the quadratic terms in $\bar{n}_\alpha$ such that $\mathcal{F}_q \approx \mathcal{F}_w$, as we see in Fig. 2(c). At low values of g, the wave model results in antibunching as $\mathcal{F}_w$ drops below 1 when $\bar{n}_h\bar{n}_c < \bar{n}_h - \bar{n}_c$. In this regime, vacuum fluctuations are crucial to capture the correct statistics, which never show antibunching in this quantum model.

Equations (10a) and (10c) readily give $\delta\mathcal{F}_{qp} = (\mathcal{S}_p - \mathcal{S})/(\langle P\rangle\Delta) \geqslant 0$, implying reduced bunching for the particle model. This can be seen in the red-shade regions in Figs. 2(b) and 2(c): For $g/\kappa \approx 2/3$, $\delta\mathcal{F}_{qp}$ has a maximum, but the particle model still has $\mathcal{F}_p \geqslant 1$. In contrast, in the limits $g/\kappa \to 0\,(\infty)$, $\delta\mathcal{F}_{qp} = 0$, independently of the temperatures.

Jointly analyzing quantum, wave, and particle models, we conclude that for low temperatures, $\bar{n}_\alpha \lesssim 1$, and $g/\kappa \approx 2/3$, neither the wave model nor the particle model captures the quantum, bosonic, noise encoded in power statistics. Therefore, even a minimal quantum heat engine, once operated in the quantum regime, contains complementary equilibrium and nonequilibrium effects stemming from wavelike and particlelike behavior. As we have shown, this is, however, not conflicting with two possible classical pictures emerging in different parameter regimes.

Thermodynamic uncertainty relations. In stochastic thermodynamics, the trade-off between power and noise has a well-established bound in terms of the entropy production rate, $\dot{\sigma}$ [46–48]. In contrast to fermionic systems, where the effect of quantum coherence can decrease noise [15], the so-called thermodynamic uncertainty relation (TUR), $\langle\langle P^2\rangle\rangle/\langle P\rangle^2 \geqslant 2/\dot{\sigma}$, cannot be violated in our bosonic model [49], and this bound immediately applies to the rate equation (8). For the power of our heat engine, the TUR is equivalent to a bound on the Fano factor, $\mathcal{F} \geqslant 2(\Omega_c/T_c - \Omega_h/T_h)^{-1}$ [solid gray curve in Fig. 2(c)]. The wave model violates this bound, and the violation coincides with the spurious antibunching. The reason for TUR violations in the wave model is the choice of the classical white noise in Eq. (7). In classical Langevin equations, the strength of the white noise is given by $k_B T_\alpha$ instead of $\bar{n}_\alpha$, which only coincide for large temperatures. Since classical Langevin equations obey the TUR [50], a modified bound holds for the wave model, $\mathcal{F}_w \geqslant 2(\bar{n}_h^{-1} - \bar{n}_c^{-1})^{-1}$ [solid purple curve in Fig. 2(c)].

Alternative classical models. The particle and wave models aforementioned are in principle not unique. In the particle model, for instance, we chose $\Gamma_I = 4g^2/(\kappa_h + \kappa_c)$. This choice is motivated because it is the only one that reproduces the quantum average power. For the wave model, a different value for the strength of the white noise [cf. Eq. (7)] could be chosen. Indeed, setting $\langle\xi^*_{\alpha,\mathrm{in}}(t')\xi_{\beta,\mathrm{in}}(t)\rangle_w = (\bar{n}_\alpha + C)\delta_{\alpha\beta}\delta(t'-t)$, with the *same* C for $\alpha = h, c$, leaves the average power (9) unchanged. Tuning C, we can attempt to account for vacuum fluctuations in the wave model; this has the consequence of modifying the equilibrium part of Eq. (10b) as $\bar{n}_\alpha^2 \to (\bar{n}_\alpha + C)^2$, which should be compared with $\bar{n}_\alpha(\bar{n}_\alpha + 1)$ in the quantum model [see Eq. (10a)]. For $C = 1/2$, the modified wave model captures the linear terms in $\bar{n}_\alpha$ present in Eq. (10a). However, for *any* $C \neq 0$, the modified wave model predicts noise at $\bar{n}_h = \bar{n}_c = 0$ and thus cannot correctly reproduce vacuum fluctuations for arbitrary temperatures.

Conclusions and outlook. We have shown that the wave-particle duality (WPD) plays a fundamental role in the power statistics of quantum heat engines. We considered a minimal model where, despite the presence of quantum coherence and vacuum fluctuations, two classical descriptions based on either particles or waves reproduce the average power of the quantum model. Power fluctuations, however, contain contributions from vacuum fluctuations and coherence which cannot be reproduced by our wave and particle models, respectively. Our work thus highlights the connection between power statistics and the WPD, a cornerstone of quantum theory. Thereby, we provide an alternative perspective for understanding engines in the quantum regime.

We stress that our approach of comparing a quantum model with a wave model and a particle model may readily be

extended to different systems and thereby opens up an alternative avenue for determining nonclassical behavior. For instance, quantum few-level systems and qubits can be contrasted with either classical few-level systems (particlelike models) or classical magnets with oscillating magnetization (wavelike models). Furthermore, by considering the full Josephson interaction in a circuit QED implementation of the heat engine considered here [26], the WPD can be exploited in a richer model which contains squeezing and non-Gaussian effects in the power statistics.

Acknowledgments. We acknowledge fruitful discussions with G. Landi and J. Rabin, and we acknowledge A. Tettamanti for carefully reading the manuscript. This work was supported by the Swiss National Science Foundation (Eccellenza Professorial Fellowship No. PCEFP2_194268).

[1] A. Einstein, On a heuristic point of view concerning the production and transformation of light, Ann. Phys. (Berlin) **322**, 132 (1905).

[2] A. Einstein, On the present status of the radiation problem, Phys. Z. **10**, 185 (1909).

[3] S. Weinberg, *Lectures on Quantum Mechanics*, 2nd ed. (Cambridge University Press, Cambridge, 2015).

[4] A. H. Compton, A quantum theory of the scattering of x-rays by light elements, Phys. Rev. **21**, 483 (1923).

[5] C. Davisson and L. H. Germer, Diffraction of electrons by a crystal of nickel, Phys. Rev. **30**, 705 (1927).

[6] W. D. Oliver, J. Kim, R. C. Liu, and Y. Yamamoto, Hanbury Brown and Twiss-type experiment with electrons, Science **284**, 299 (1999).

[7] W. K. Wootters and W. H. Zurek, Complementarity in the double-slit experiment: Quantum nonseparability and a quantitative statement of Bohr's principle, Phys. Rev. D **19**, 473 (1979).

[8] B.-G. Englert, Fringe visibility and which-way information: An inequality, Phys. Rev. Lett. **77**, 2154 (1996).

[9] C. Dittel, G. Dufour, G. Weihs, and A. Buchleitner, Wave-particle duality of many-body quantum states, Phys. Rev. X **11**, 031041 (2021).

[10] K. Wang, Q. Xu, S. Zhu, and X.-s. Ma, Quantum wave-particle superposition in a delayed-choice experiment, Nat. Photonics **13**, 872 (2019).

[11] M. T. Mitchison, M. P. Woods, J. Prior, and M. Huber, Coherence-assisted single-shot cooling by quantum absorption refrigerators, New J. Phys. **17**, 115013 (2015).

[12] S. Nimmrichter, J. Dai, A. Roulet, and V. Scarani, Quantum and classical dynamics of a three-mode absorption refrigerator, Quantum **1**, 37 (2017).

[13] A. A. S. Kalaee, A. Wacker, and P. P. Potts, Violating the thermodynamic uncertainty relation in the three-level maser, Phys. Rev. E **104**, L012103 (2021).

[14] K. Korzekwa and M. Lostaglio, Quantum advantage in simulating stochastic processes, Phys. Rev. X **11**, 021019 (2021).

[15] K. Prech, P. Johansson, E. Nyholm, G. T. Landi, C. Verdozzi, P. Samuelsson, and P. P. Potts, Entanglement and thermokinetic uncertainty relations in coherent mesoscopic transport, Phys. Rev. Res. **5**, 023155 (2023).

[16] W. G. Unruh and W. H. Zurek, Reduction of a wave packet in quantum Brownian motion, Phys. Rev. D **40**, 1071 (1989).

[17] W. H. Zurek, S. Habib, and J. P. Paz, Coherent States via Decoherence, Phys. Rev. Lett. **70**, 1187 (1993).

[18] W. H. Zurek, Decoherence, einselection, and the quantum origins of the classical, Rev. Mod. Phys. **75**, 715 (2003).

[19] R. W. Spekkens, Evidence for the epistemic view of quantum states: A toy theory, Phys. Rev. A **75**, 032110 (2007).

[20] R. W. Spekkens, Quasi-quantization: Classical statistical theories with an epistemic restriction, in *Quantum Theory: Informational Foundations and Foils*, edited by G. Chiribella and R. W. Spekkens (Springer, Dordrecht, 2016), pp. 83–135.

[21] A. W. Harrow and A. Montanaro, Quantum computational supremacy, Nature (London) **549**, 203 (2017).

[22] L. Mandel, Non-classical states of the electromagnetic field, Phys. Scr. **T12**, 34 (1986).

[23] A. Ghosh, W. Niedenzu, V. Mukherjee, and G. Kurizki, Thermodynamic principles and implementations of quantum machines, in *Thermodynamics in the Quantum Regime: Fundamental Aspects and New Directions*, edited by F. Binder, L. A. Correa, C. Gogolin, J. Anders, and G. Adesso (Springer International, Cham, Switzerland, 2018), pp. 37–66.

[24] T. Kerremans, P. Samuelsson, and P. Potts, Probabilistically violating the first law of thermodynamics in a quantum heat engine, SciPost Phys. **12**, 168 (2022).

[25] R. Kosloff, A quantum mechanical open system as a model of a heat engine, J. Chem. Phys. **80**, 1625 (1984).

[26] P. P. Hofer, J.-R. Souquet, and A. A. Clerk, Quantum heat engine based on photon-assisted Cooper pair tunneling, Phys. Rev. B **93**, 041418(R) (2016).

[27] R. Alicki and R. Kosloff, Introduction to quantum thermodynamics: History and prospects, in *Thermodynamics in the Quantum Regime: Fundamental Aspects and New Directions*, edited by F. Binder, L. A. Correa, C. Gogolin, J. Anders, and G. Adesso (Springer International, Cham, Switzerland, 2018), pp. 1–33.

[28] M. Westig, B. Kubala, O. Parlavecchio, Y. Mukharsky, C. Altimiras, P. Joyez, D. Vion, P. Roche, D. Esteve, M. Hofheinz, M. Trif, P. Simon, J. Ankerhold, and F. Portier, Emission of nonclassical radiation by inelastic Cooper pair tunneling, Phys. Rev. Lett. **119**, 137001 (2017).

[29] A. Peugeot, G. Ménard, S. Dambach, M. Westig, B. Kubala, Y. Mukharsky, C. Altimiras, P. Joyez, D. Vion, P. Roche, D. Esteve, P. Milman, J. Leppäkangas, G. Johansson, M. Hofheinz, J. Ankerhold, and F. Portier, Generating two continuous entangled microwave beams using a dc-biased Josephson junction, Phys. Rev. X **11**, 031008 (2021).

[30] G. C. Menard, A. Peugeot, C. Padurariu, C. Rolland, B. Kubala, Y. Mukharsky, Z. Iftikhar, C. Altimiras, P. Roche, H. L. Sueur, P. Joyez, D. Vion, D. Esteve, J. Ankerhold, and F. Portier, Emission of Photon Multiplets by a dc-Biased Superconducting Circuit, Phys. Rev. X **12**, 021006 (2022).

[31] M. Aspelmeyer, T. J. Kippenberg, and F. Marquardt, Cavity optomechanics, Rev. Mod. Phys. **86**, 1391 (2014).

[32] J. Monsel, N. Dashti, S. K. Manjeshwar, J. Eriksson, H. Ernbrink, E. Olsson, E. Torneus, W. Wieczorek, and J. Splettstoesser, Optomechanical cooling with coherent and squeezed light: The thermodynamic cost of opening the heat valve, Phys. Rev. A **103**, 063519 (2021).

[33] See Supplemental Material at http://link.aps.org/supplemental/10.1103/PhysRevResearch.5.L042007 for detailed calculations of the average current and noise in each model and a short note on the connection between power and work variance.

[34] C. W. Gardiner and M. J. Collett, Input and output in damped quantum systems: Quantum stochastic differential equations and the master equation, Phys. Rev. A **31**, 3761 (1985).

[35] C. W. Gardiner and P. Zoller, *Quantum Noise: A Handbook of Markovian and Non-Markovian Quantum Stochastic Methods With Applications to Quantum Optics* (Springer, New York, 2004).

[36] P. A. Franken, A. E. Hill, C. W. Peters, and G. Weinreich, Generation of optical harmonics, Phys. Rev. Lett. **7**, 118 (1961).

[37] Y. V. G. S. Murti and C. Vijayan, A phenomenological view of nonlinear optics, in *Physics of Nonlinear Optics* (Springer International, Cham, Switzerland, 2021), pp. 9–25.

[38] C. W. Gardiner, *Handbook of Stochastic Methods: For Physics, Chemistry and the Natural Sciences* (Springer, New York, 2004).

[39] L. Isserlis, On a formula for the product-moment coefficient of any order of a normal frequency distribution in any number of variables, Biometrika **12**, 134 (1918).

[40] C. Flindt, T. Novotny, A. Braggio, and A.-P. Jauho, Counting statistics of transport through Coulomb blockade nanostructures: High-order cumulants and non-Markovian effects, Phys. Rev. B **82**, 155407 (2010).

[41] Y. Blanter and M. Büttiker, Shot noise in mesoscopic conductors, Phys. Rep. **336**, 1 (2000).

[42] A. A. Clerk, M. H. Devoret, S. M. Girvin, F. Marquardt, and R. J. Schoelkopf, Introduction to quantum noise, measurement, and amplification, Rev. Mod. Phys. **82**, 1155 (2010).

[43] F. Brange, P. Menczel, and C. Flindt, Photon counting statistics of a microwave cavity, Phys. Rev. B **99**, 085418 (2019).

[44] L. Basano, P. Ottonello, and B. Torre, Bunching, antibunching, and the Poisson limit of Bose-Einstein processes at low-degeneracy parameters, J. Opt. Soc. Am. B **22**, 1314 (2005).

[45] A. Kronwald, M. Ludwig, and F. Marquardt, Full photon statistics of a light beam transmitted through an optomechanical system, Phys. Rev. A **87**, 013847 (2013).

[46] A. C. Barato and U. Seifert, Thermodynamic uncertainty relation for biomolecular processes, Phys. Rev. Lett. **114**, 158101 (2015).

[47] T. R. Gingrich, J. M. Horowitz, N. Perunov, and J. L. England, Dissipation bounds all steady-state current fluctuations, Phys. Rev. Lett. **116**, 120601 (2016).

[48] J. M. Horowitz and T. R. Gingrich, Thermodynamic uncertainty relations constrain non-equilibrium fluctuations, Nat. Phys. **16**, 15 (2020).

[49] S. Saryal, H. M. Friedman, D. Segal, and B. K. Agarwalla, Thermodynamic uncertainty relation in thermal transport, Phys. Rev. E **100**, 042101 (2019).

[50] T. R. Gingrich, G. M. Rotskoff, and J. M. Horowitz, Inferring dissipation from current fluctuations, J. Phys. A: Math. Theor. **50**, 184004 (2017).